Mattern, Anne; Sandig, Romy; Joos, Alexander; Löwa, Norbert; Kosch, Olaf; Weidner, Andreas; Wells, James; Wiekhorst, Frank; Dutz, Silvio:

Magnetic nanoparticle-gel materials for development of joint phantoms for MPI and MRI

Original published in:	International journal on magnetic particle imaging. - Lübeck : Infinite Science Publishing. - 4 (2018), 2, art. 1811001, 5 pp.
Original published:	2019-03-05
ISSN:	2365-9033
DOI:	10.18416/ijmpi.2018.1811001
[*Visited:*	2020-01-28]

International Journal on Magnetic Particle Imaging
Vol 4, No 2, Article ID 1811001, 5 Pages

Infinite Science Publishing

Research Article

Magnetic Nanoparticle-Gel Materials for Development of Joint Phantoms for MPI and MRI

Anne Mattern[a] · Romy Sandig[a] · Alexander Joos[b,c] · Norbert Löwa[b] · Olaf Kosch[b] · Andreas Weidner[a] · James Wells[b] · Frank Wiekhorst[b] · Silvio Dutz[a,*]

[a] Institute of Biomedical Engineering and Informatics, Technische Universität Ilmenau, Ilmenau, Germany
[b] Physikalisch-Technische Bundesanstalt, Berlin, Germany
[c] Munich School of BioEngineering, Technical University of Munich, Garching, Germany
*Corresponding author, email: silvio.dutz@tu-ilmenau.de

Received 24 November 2016; Accepted 12 September 2018; Published online 08 November 2018

Abstract

To evaluate the performance of commercial as well as custom-made scanners, dedicated phantoms with defined magnetic nanoparticle (MNP) distributions are required. Prerequisite for the development of such phantoms is the establishment of suitable MNP-matrix combinations. In this study, two different gel types were investigated as potential matrix materials: water-based biopolymers and synthetic polymers. These materials exhibit similar imaging behaviour to body tissue in MRI and MPI. Aqueous suspensions of MNP coated with different types of functionalized dextranes were used for embedding particles into the biopolymers, and organic fluids with oleic acid coated MNP for synthetic polymers, respectively. The obtained MNP-matrix combinations were tested for their shape stability. The homogeneity of MNP distribution and immobilization within the matrix was determined by optical investigation of the samples with a microscope, and the magnetic properties of the composite materials measured by vibrating sample magnetometry. From the tested combinations of MNP and matrix material, oleic acid coated MNP embedded in Permagel was found to be the most suitable for the construction of MPI phantoms. This was based on the reliable and homogeneous fixation of the MNP within the matrix without agglomeration of the particles.

I. Introduction

Since the first description of the MPI principle in 2005 [1], a variety of different laboratory MPI scanners are present in laboratories all over the world [2]. In 2014, the first commercial scanner was brought onto the market by Bruker BioSpin. These scanners enable the reconstruction of the spatial distribution of magnetic nanoparticles (MNP) within tissue, which is of major importance for many applications of MNP in biomedicine [3, 4].

To enable researchers to explore the potential of this promising novel imaging modality, the detection limits and image resolutions of the present MPI scanners have to be assessed as a benchmark for potential applications. Therefore, well-defined and comparable magnetic structures are needed to perform comparison studies between different MPI set-ups. Furthermore, because MPI depicts only the spatial distribution of MNP, applications typically require a co-registration with another imaging

modality (e.g. CT or MRI) to correlate the particles' pattern with morphological structures within the body. For this reason, phantoms which are suitable for use in both MPI and MRI scanners are highly advantageous.

Up to now, each laboratory uses its own measurement phantoms [5–9]. Mostly, these phantoms consist of MNP within a liquid at a certain concentration, filled into containers of different volume. Such liquid phantoms often exhibit poor long-term stability, and thus do not allow ring-test studies between different labs, or the monitoring of MPI scanner stability over time.

In this study, materials were developed for the construction of dedicated phantoms to monitor and assess relevant imaging properties of an MPI scanner.

The first objective of the study was to identify gel materials suitable for use as a phantom matrix, enabling the preparation of mechanically long-term stable phantoms. The secondary goal was to find coating materials which enable the agglomeration-free embedding of magnetic particles within this matrix. Furthermore, the phantom materials should be able to be imaged by means of MRI for a possible co-registration of MPI and MRI data.

The main requirements for an optimal combination of MNP and matrix are good imaging properties of the MNPs used, and a homogeneous and agglomeration-free distribution of these particles within the matrix. Ideally, this matrix should be long-term stable, and guarantee a constant imaging quality of the completed phantom over a long period. In 2017 Lüdtke-Buzug et al. presented MNP-doped PLA based polymers with promising magnetic and mechanical properties for MPS/MPI [10]. There, the MNP are embedded into the matrix during the synthesis of the PLA. In our approach, we focus on commercially available matrix materials, which can be blended with various MNP. For this, a multitude of combinations of magnetic nanoparticles (with different coatings) and several matrix materials (water-based biopolymers as well as synthetic silicone) were tested for their suitability for the preparation of dedicated measurement phantoms.

The most promising material combinations are utilized for the preparation of measurement phantoms with defined structures and concentrations as well as more realistic phantoms, which simulate the particle behavior within animals or tissue. These phantoms will be made available to scientists who are working with MPI scanners to explore the potential of the promising MPI technique. Consequently, also the number of required animal testing can be reduced by using phantoms close to reality for comparative studies.

II. Methods

II.I. Preparation of ferrofluids

Aqueous suspensions (ferrofluids) of MNP were prepared as described before [11]. In short: a 1 M $NaHCO_3$ solution was slowly added to a $FeCl_2/FeCl_3$ solution (total Fe-concentration: 1.25 M; Fe^{2+}/Fe^{3+} ratio = 1/1.3) at a rate of 0.75 ml/min under permanent stirring up to pH = 8, leading to the formation of a brownish precipitate. Afterwards, the solution was boiled for 5 minutes to form an almost black precipitate. Then, the magnetic nanoparticles were washed with water. To produce sedimentation stable suspensions, the bare particles (PUR) were stabilized with different types of coatings. Thus, we obtained MNP coated by carboxymethyl dextran (CMD), dextran (DEX), aminodextran (DEAE), and oleic acid (OA) shell. The MNP concentration in the suspension was adjusted to a value of about 1.5 % by mass (c_{Fe} about 1.0 %).

II.II. Combinations of gels and MNP

As matrix materials, two different types of gels were used:

(i) water based biopolymers
(ii) synthetic polymers

The water-based biopolymers (i) studied were:

- agarose (Ag)
- agar agar (AA)
- gelatine (Gel)
- ballistic gel (BG)
- a gelatin-oil mixture (GelOl)
- a gelatin-oil-formaldehyte mixture (GelOlF)

The synthetic polymers (ii) employed were:

- Elastosil
- Permagel
- silicone rubber

All matrix materials were mixed with the prepared ferrofluids at a matrix/fluid ratio of 9/1 by volume to obtain a MNP loaded matrix for the preparation of measuring objects within the phantom. For this, the MNP were added to the matrix material and stirred mechanically for one minute.

II.III. Characterization

All materials were tested for their long-term and shape stability as well as for their magnetic and MR imaging behavior. Therefore, test bodies of all matrix materials at different concentrations were molded into cylindrical shapes ($D = 25\,\text{mm}$, $H = 50\,\text{mm}$). Over a period of 4 weeks, the test bodies were stored at a temperature of 20 °C and a humidity of 50 ± 10 %. During this time interval, changes in the shape of the test bodies were investigated visually.

10.18416/ijmpi.2018.1811001

Table 1: MNP concentrations of serial dilution.

Sample no.	Concentration [mmol/L]
1	0.1
2	0.25
3	0.5
4	1
5	2.5
6	5
7	10

The MRI imaging behavior of the plain matrix materials was investigated by means of a 1 T preclinical MRI scanner (Bruker ICON). For this, MRI images of cylindrically shaped test bodies were acquired using a 2D spin echo sequence with the following parameters: matrix size = 192 × 192, field of view (FOV) = 49 × 49 mm^2, slice thickness (TH) = 1 mm, 2 averages, repetition time (TR) = 1 s, echo time (TE) = 8 ms for the most promising materials. It was tested, if the plain matrix material can be imaged in MRI and if it is possible to distinguish between different matrix materials (by different relaxivities) when imaging them simultaneously. To evaluate which concentration of MNP is necessary to get an appropriate imaging result in MPI and MRI, a serial dilution was measured. For this purpose, matrix materials with defined MNP concentrations between 0.1 and 10.0 mmol/L were prepared (Table 1) and MRI images were acquired using a 2D multi-spin multi-echo sequence with the following parameters: matrix size = 256 × 128, FOV = 80 × 40 mm^2, TH: 1 mm, 4 averages, TR = 3 s, TE = 5 ms (first echo). Since MPI needs high MNP concentrations for a reliable reconstruction, the dilution series was also imaged with MRI using a 3D ultrashort TE (UTE) sequence with the following parameters: FOV 50 × 50 × 50 mm^3, TE = 0.01 ms, TR = 5 ms, flip angle = 5°. UTE sequences allow for extremely short echo times below 1 ms, and thus enable the detection of signals from samples with high MNP concentration that exhibit a very short transverse relaxation time. After acquisition, the spin-echo and UTE images were visually inspected to determine whether the signal of individual samples was strong enough to discriminate them clearly from background noise. To evaluate the distribution of the MNP within the matrix materials, the MNP-Gel combinations were investigated by optical microscopy. Furthermore, from these investigations the occurrence of MNP agglomerates within the gel matrix could be determined. To get information on the degree of attachment of the MNP within the matrix, the samples were investigated by vibrating sample magnetometry (VSM). As a measure for the attachment, we determined the ratio between coercivity of MNP within the gel with coercivity of the same sample after drying it on blotting paper (LP).

To analyze the MPI performance of the MNP loaded matrices, we used a commercial preclinical MPI scanner (MPI 25/20 FF, Bruker BioSpin). This field-free-point (FFP) scanner uses the system function approach for image reconstruction. The spatial encoding was achieved by field gradients of 1.25 T/m in z-direction and 0.625 T/m in x- and y-direction. During measurement, the FFP is moved on a closed 3D Lissajous-trajectory through the FOV (38.4 × 38.4 × 19.2 mm^3) by applying three orthogonal drive-fields of 12 mT amplitude. Finally, we used all frequency components with an SNR threshold larger than five. Images were obtained using the Kaczmarz algorithm with 5 iterations and a relative regularization parameter of 10^{-5}.

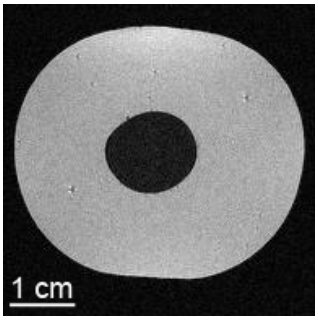

Figure 1: MRI cross section image of an Elastosil cylinder embedded into Permagel using a 2D spin echo sequence (FOV = 49 × 49 mm^2, TH = 1 mm, 2 averages, TR = 1 s, TE = 8 ms).

II.IV. Preparation of a phantom

From the most promising material combinations, a measurement phantom was built up and imaged by means of MRI and MPI. For this, three cylindrically shaped objects (D=H: 14, 9, and 6 mm) consisting of oleic acid coated MNP embedded into Permagel with a concentration of 5 mmol(MNP)/L were prepared and embedded into a second matrix of Elastosil, to stabilize the arrangement of the three cylinders mechanically.

III. Results

The visual investigation of the long-term stability of the investigated matrix materials showed, that all biopolymers exhibit a poor shape stability of just a few days.

After this time the matrix starts to shrink as a result of drying, which leads to a deformation of the test bodies. Furthermore, when drying of the test bodies was prevented, a microbial contamination of the materials was observed after about two weeks. Therefore, these materials have a limited durability of only some days and show no long-term stability. Compared to this, all synthetic polymers investigated show a long-term stability with no deformation or contamination over the complete time of the study (six months). For the plain matrix materials

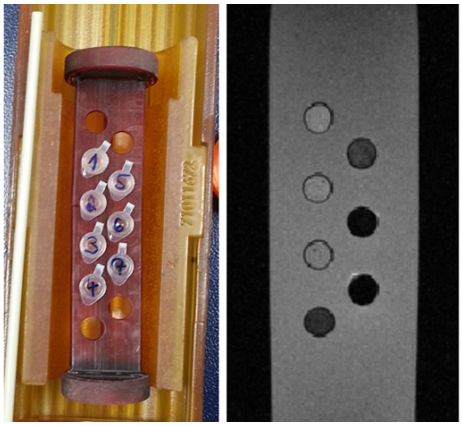

Figure 2: Sample holder with serial dilution of oleic acid coated MNP embedded in Permagel (left) and MRI multi-echo images (right; FOV = 80 × 40 mm^2, TH = 1 mm, 4 averages, TR = 3 s, TE = 5 ms).

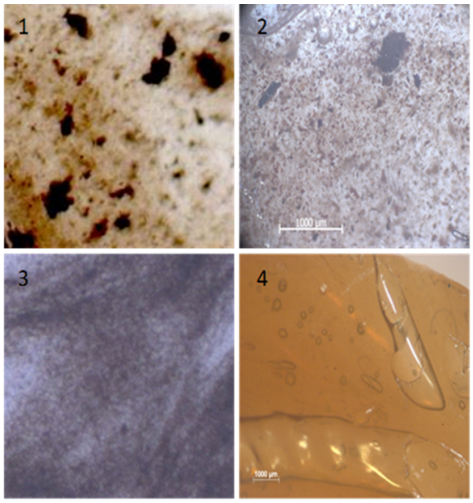

Figure 3: Microscope images of DEAE in GelOl (1), uncoated MNP (PUR) in Permagel (2), CMD in BG (3), and OA coated MNP in Permagel (4).

measured in MRI, all biopolymers as well as Permagel and Elastosil were found to produce enough signal for reliable imaging of objects by MRI. Note, that the MRI signal is determined by both the concentration of hydrogen atoms and the relaxation times.

As an example, Figure 1 shows an MRI image of an Elastosil cylinder embedded into Permagel. Silicon rubber objects could not be imaged by MRI due to insufficient signal. Therefore, this material was excluded from further investigations, but might be interesting for the preparation of MPI phantoms without a necessary co-registration by means of MRI.

For MRI imaging of the MNP serial dilution, a maximum MNP concentration of 2.5 mmol/L seems to be promising, while at higher MNP concentrations the relaxation times are too short for the signal to be detected

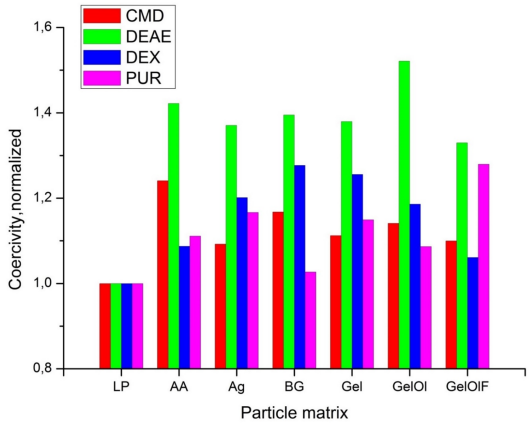

Figure 4: Coercivity ratio (coercivity normalized to the value for blotting paper (LP)) of different MNP/Biopolymer combinations.

using a standard spin echo sequence (see samples 6 and 7 in Figure 2).

Microscopy on biopolymers containing CMD and dextran coated as well as uncoated (PUR) MNP revealed a homogeneous MNP distribution of most of the investigated MNP-gel combinations. A strong agglomeration was observed for the DEAE MNP in all biopolymers, e.g. see Figure 3.1. For the biopolymers, the most homogeneous and agglomeration free mixture was obtained for CMD-MNP in ballistic gel, see picture 3 in Figure 3.

Microscopic inspection of the synthetic polymers containing MNP revealed a poor distribution for almost all of the coated particles. Also, a strong agglomeration was observed for embedding uncoated MNP (PUR) into all synthetic polymers, e.g. see picture 2 in Figure 3. Only oleic acid coated particles dispersed in dodecane showed a homogeneous and agglomeration free distribution of particles within Permagel, see picture 4 in Figure 3. Therefore, for synthetic polymers, VSM measurements were performed for oleic acid coated MNP embedded into Permagel only.

Figure 4 shows the coercivity ratio between MNP embedded in biopolymers and MNP immobilized on blotting paper, determined by VSM measurements. Strong variations in the coercivity ratio are clearly seen. All combinations show an attachment of the MNP within the matrix (coercivity ratio in the range of 1 to 1.2), but for some combinations a strong agglomeration is found (e.g. all DEAE combinations), which is indicated by a very high coercivity ratio.

For the VSM investigation of oleic acid coated MNP within Permagel, no significant difference in coercivity compared to these particles immobilized on blotting paper was found.

The MR imaging of a phantom containing oleic acid coated MNP embedded into Permagel was successful using the UTE sequence (see Figure 5.1). All three particle-

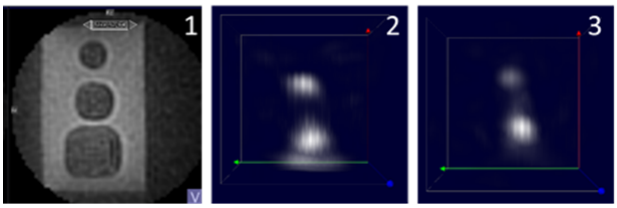

Figure 5: MRI image (1) of the 14 mm, 9 mm and 6 mm cylinder using a 3D UTE sequence (FOV $50 \times 50 \times 50\,mm^3$, TE = 0.01 ms, TR = 5 ms, flip angle = 5°). For MPI only two cylinders could be visualized simultaneously due to the smaller FOV ($38.4 \times 38.4 \times 19.2\,mm^3$). Shown are intensity value images from an MPI scan of a 14 mm and 9 mm cylinder (2) as well as of a 9 mm and 6 mm cylinder (3).

loaded cylinders can be detected in the scan. In contrast, due to the smaller FOV, only two cylinders could be visualized in one scan by means of MPI (see Figure 5.2 and Figure 5.3). However, all three differently sized cylinders were clearly visible in MPI.

IV. Conclusion

When looking at the results for shape stability tests, MNP distribution, agglomeration, and attachment, the most promising combination for MNP embedded into biopolymers are CMD coated MNP embedded in ballistic gel. BG shows the best shape stability of investigated biopolymers, even if the long-term stability is relatively low, compared to those of synthetic polymers. The most homogeneous particle distribution in BG was obtained for CMD particles (see picture 3 in Figure 3) and the VSM measurements confirm by a relatively low coercivity ratio a slight agglomeration only. Figure 4 shows that other combinations show lower or similar agglomeration than for CMD particles in BG, but these material combinations show clear drawbacks regarding shape stability of the matrix and particle distribution within the matrix.

For the synthetic polymers, the most promising results from all measurements were obtained for oleic acid coated MNP embedded in Permagel. This material combination is long-term stable regarding shape stability, shows a homogeneous and agglomeration free particle distribution and a good particle attachment within the matrix.

From the latter combination, measurement phantoms were successfully constructed and imaged using both MRI and MPI successfully.

In ongoing studies, better magnetic cores have to be used to obtain a higher spatial resolution, which is a requirement for the manufacture and successful imaging of more realistically shaped measurement phantoms, e.g. a reproduction of parts of the vascular systems with very small structures (capillaries).

Acknowledgements

The authors thank M.Sc. Mathias Fritz (TU Ilmenau) for assistance during microscopy. This work was supported by Deutsche Forschungsgemeinschaft (FKZ: DU 1293/6-1 and TR408/9-1). The authors acknowledge support for the Article Processing Charge by the German Research Foundation (DFG) and the Open Access Publication Fund of the Technische Universität Ilmenau.

References

[1] B. Gleich and J. Weizenecker. Tomographic imaging using the nonlinear response of magnetic particles. *Nature*, 435(7046):1214–1217, 2005, doi:10.1038/nature03808.

[2] N. Panagiotopoulos, F. Vogt, J. Barkhausen, T. M. Buzug, R. L. Duschka, K. Lüdtke-Buzug, M. Ahlborg, G. Bringout, C. Debbeler, M. Gräser, C. Kaethner, J. Stelzner, H. Medimagh, and J. Haegele. Magnetic particle imaging: current developments and future directions. *International Journal of Nanomedicine*, 10(1):3097–3114, 2015, doi:10.2147/IJN.S70488.

[3] K. M. Krishnan. Biomedical Nanomagnetics: A Spin Through Possibilities in Imaging, Diagnostics, and Therapy. *IEEE Transactions on Magnetics*, 46(7):2523–2558, 2010, doi:10.1109/TMAG.2010.2046907.

[4] Q. A. Pankhurst, N. T. K. Thanh, S. K. Jones, and J. Dobson. Progress in applications of magnetic nanoparticles in biomedicine. *Journal of Physics D: Applied Physics*, 42(22):224001, 2009, doi:10.1088/0022-3727/42/22/224001.

[5] R. M. Ferguson, A. P. Khandhar, S. J. Kemp, H. Arami, E. U. Saritas, L. R. Croft, J. Konkle, P. W. Goodwill, A. Halkola, J. Rahmer, J. Borgert, S. M. Conolly, and K. M. Krishnan. Magnetic Particle Imaging With Tailored Iron Oxide Nanoparticle Tracers. *IEEE Transactions on Medical Imaging*, 34(5):1077–1084, 2015, doi:10.1109/TMI.2014.2375065.

[6] K. Gräfe, G. Bringout, M. Graeser, T. F. Sattel, and T. M. Buzug. System Matrix Recording and Phantom Measurements with a Single-Sided Magnetic Particle Imaging Device. *IEEE Transactions on Magnetics*, 51(2):1–3, 2015, doi:10.1109/TMAG.2014.2330371.

[7] T. Knopp and T. M. Buzug, Magnetic Particle Imaging: An Introduction to Imaging Principles and Scanner Instrumentation. Berlin, Heidelberg: Springer Berlin Heidelberg, 2012, doi:10.1007/978-3-642-04199-0.

[8] J. J. Konkle, P. W. Goodwill, O. M. Carrasco-Zevallos, and S. M. Conolly. Projection Reconstruction Magnetic Particle Imaging. *IEEE Transactions on Medical Imaging*, 32(2):338–347, 2013, doi:10.1109/TMI.2012.2227121.

[9] S. Vaalma, J. Rahmer, N. Panagiotopoulos, R. L. Duschka, J. Borgert, J. Barkhausen, F. M. Vogt, and J. Haegele. Magnetic Particle Imaging (MPI): Experimental Quantification of Vascular Stenosis Using Stationary Stenosis Phantoms. *PLOS ONE*, 12(1):e0168902B. Xu, Ed., 2017, doi:10.1371/journal.pone.0168902.

[10] C. Jacobi, T. Friedrich, and K. Lüdtke-Buzug. Synthesis and Characterisation of Superparamagnetic Polylactic acid based Polymers. *International Journal on Magnetic Particle Imaging*, 3(2), 2017, doi:10.18416/ijmpi.2017.1710001.

[11] S. Dutz, J. H. Clement, D. Eberbeck, T. Gelbrich, R. Hergt, R. Müller, J. Wotschadlo, and M. Zeisberger. Ferrofluids of magnetic multicore nanoparticles for biomedical applications. *Journal of Magnetism and Magnetic Materials*, 321(10):1501–1504, 2009, doi:10.1016/j.jmmm.2009.02.073.

